J Mol Model (2013) 19:4511–4519
DOI 10.1007/s00894-013-1962-1

ORIGINAL PAPER

Single crystal architecture and absorption spectra of octathio[8]circulene and *sym*-tetraselenatetrathio[8]circulene: QTAIM and TD-DFT approach

Gleb V. Baryshnikov · Boris F. Minaev · Valentina A. Minaeva · Valentine G. Nenajdenko

Received: 24 June 2013 / Accepted: 24 July 2013 / Published online: 14 August 2013

Abstract The single crystal architecture of the high-symmetry octathio[8]circulene and *sym*-tetraselenatetrathio[8]circulene is studied at the density functional theory (DFT) level with the quantum theory of atoms in molecules (QTAIMs) approach to the electron density distribution analysis. The presence of stabilizing intermolecular C–-C, C–-S and C–-Se contacts in the longitudinal and transversal projections of the single crystals is postulated on the grounds of the previous high-resolution X-ray data for octathio[8]circulene; it is supported by the present QTAIM calculations and also predicted in some new details for both circulenes. We suggest that the appearance of the observed red color for the monocrystalline octathio[8]circulene is caused by strong intermolecular interactions between the molecules in the single crystal. However, the intermolecular interactions for the *sym*-tetraselenatetrathio[8]circulene crystal fragment are weaker and molecular layers are more friable in comparison to octathio[8]circulene crystal structure. These lead to the absence of visible absorption for the *sym*-tetraselenatetrathio[8]circulene crystal.

Keywords Absorption spectra · Bader's theory · Non-covalent interactions · Octathio[8]circulene · Single crystal

G. V. Baryshnikov (✉) · B. F. Minaev · V. A. Minaeva
Bohdan Khmelnytsky National University,
18031 Cherkassy, Ukraine
e-mail: glebchem@rambler.ru

V. G. Nenajdenko
Department of Chemistry, Moscow State University,
119992 Moscow, Russia

Introduction

Octathio[8]circulene (**C1**) [1–4], *sym*-tetraselenatetrathio[8]circulene (**C2**) [2, 3] and their heteroatomic analogues (tetraoxa[8]circulenes, azaoxa[8]circulenes etc.) [5–13] represent the condensed planar heterocyclic compounds that hold promise in microelectronics and nanophotonics. In particular, the **C1** and **C2** compounds proved to be useful for applications in organic light-emitting devices (OLEDs) [4, 6] and organic field-effect transistors (OFETs) [2, 4, 14–19]. The compounds presented in Scheme 1 are well studied by various experimental methods.

In particular, the high-resolution X-ray analysis was applied to the single crystal architecture description of the **C1** compound, including the IR, Raman and UV–vis spectra studies [20, 21]. Bukalov at el. [20] have shown that sublimation of the **C1** compound leads to formation of two modifications: a white film (**1W**) and a red polycrystalline solid (**1R**). The **1W** modification corresponds to amorphous octathio[8]circulene, but the **1R** modification consists of the well-organized stacked **C1** molecules [20]. Clearly, the different colors of the **1W** and **1R** forms are determined by different structural organization of the **C1** solid state modifications. However, the **C2** compound in the amorphous and monocrystalline states is colorless. Therefore the objective of this work is a theoretical study of the single crystal architecture and UV–vis absorption spectra of the **C1** and **C2** circulenes in order to elucidate the nature of the **C1** color and of the **C2** colorlessness. Recently the electronic structure and the vertical absorption spectrum of the **C1** molecule have been theoretically investigated by Arago et al. [22]. We have supported their results and supplemented by symmetry analysis with the spin and orbital selection rules. The theoretical description of the single crystal structure and the UV–vis spectra for the *sym*-

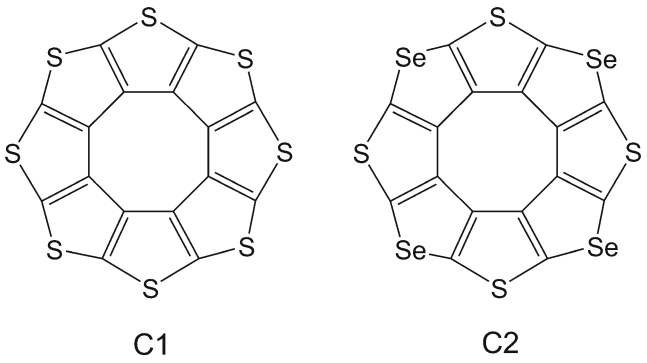

Scheme 1 Structure of the **C1** and **C2** compounds

tetraselenatetrathio[8]circulene molecule are presented here for the first time on the basis of TD DFT and QTAIM calculations.

Computational details

The input atomic coordinates of the **C1**, **C2** molecules and of their associates (dimer, tetra- and hexamer) have been taken from the high-resolution single crystal X-ray experimental data (CCDC-685932) [20]. The single point calculations at the fixed geometry for the studied systems have been performed at the DFT B3LYP/6-31G(d) level [23–25] using GAUSSIAN 03 package [26]. For the obtained Kohn-Shem orbitals a topological analysis of electron density distribution function $\rho(\mathbf{r})$ has been performed by the Bader method named "quantum theory of atoms in molecules" (QTAIMs) [27–30] with the AIMAll package [31].

The possibility to use the experimental (non-optimized by DFT) atomic coordinates for the correct QTAIM analysis have been shown previously for the different types of molecular associates [32–34]. For example, a good agreement between experimentally measured and calculated topological parameters of the $\rho(\mathbf{r})$ function for hydrated cupric acetate is shown in ref [32]. In the present work we use the additivity scheme for the separation of elementary crystal packing for the **C1** and **C2** compound to a number of the corresponding dimers. For the studied dimers an existence of intermolecular binding interactions and their electronic parameters have been determined by the QTAIM method. According to the Bader's formalism [27], the presence of the bond critical point (CP) of the (3, −1) type and the presence of bond path between the interacting atoms is the necessary and sufficient condition of existence of the interatomic binding interaction. The energy of intermolecular noncovalent contacts between the circulene molecules in the crystal packing fragments is estimated by the following equation, derived by Espinosa et al. [35, 36]:

$$E = 313.754\,\nu(\mathbf{r}), \quad (1)$$

where E is the energy of interatomic interaction (kcal mol^{-1}), $\nu(\mathbf{r})$—potential energy density (a.u.) in the corresponding critical point of the (3, −1) type. The estimation of stacking interactions energy on the basis of Espinosa equation is a normal practice in recent studies [37–39].

The electronic excited states properties of the investigated compounds have been calculated by TD DFT method [40] using B3LYP hybrid functional with the same 6-31G(d) basis set. We also have performed the detailed analysis of the **C1** and **C2** adsorption spectra with the control of their possible symmetry constrain (D_{8h} and D_{4h} for **C1** and **C2**, respectively). In this connection we have obtained the equilibrium geometries for the ground states of the studied molecules optimized with the same B3LYP/6-31G(d) method and have calculated the lowest 70 vertical singlet-singlet electronic transitions for both species. The calculations have been performed in the vacuum approximation, which corresponds to the measurement of the absorption spectra in the form of a freshly sublimed amorphous white film [20].

Results and discussion

General remarks on the C1 and C2 single crystal architecture

The structure of the **C1** and **C2** crystal packing fragments is presented in Fig. 1. Each fragment consists of six molecules being positioned in accordance to the C_i space point group. Therefore, only four types of contacts (**A1**, **A2**, **A3** and **A4**) are realized for each crystal packing fragment. The total number of contacts is distributed as the following: two **A1**-types, four both **A2**- and **A3**-types and a single **A4**-type of contacts. The **A1** dimer illustrates intracolumnar stacking interactions, while the **A2**-**A4** pairs correspond to intercolumnar noncovalent interactions (Fig. 1). The molecular fragments presented in Fig. 1 (top) illustrate the longitudinal zigzag-shaped architecture of the **C1** and **C2** single crystals. The **M1**, **M3**, **M4** and **M5** molecules presented in the bottom of Fig. 1 correspond to molecular columns (stacks) which form the transversal projection of the **C1** and **C2** single crystals.

Based on the QTAIM calculations we can assume that transversal columns are stabilized by the weak noncovalent C···C, C···S and C···Se contacts (Fig. 2); longitudinal structure of the studied crystals are also stabilized by the weak noncovalent S···S and S···Se interactions (Fig. 3). The existence of all these bond types is proved experimentally for the **C1** compound in ref [20]. At the same time some new types of noncovalent bonds are predicted by our QTAIM analysis. Thus, our theoretical calculations are directly confirmed by experiment and agree well with ref [20] on the quantitative level of topological parameters of electron density distribution function in the critical points of the (3, −1) type.

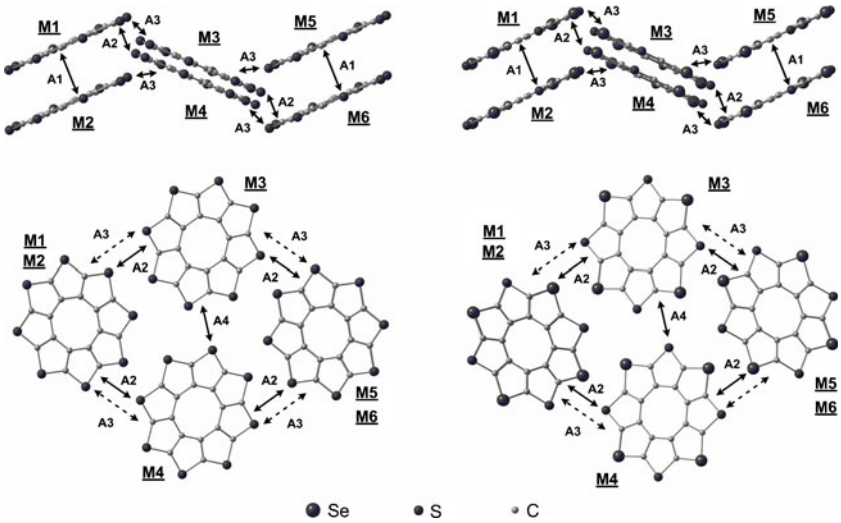

Fig. 1 Longitudinal fragments of crystal packing of the **C1** (*left*) and **C2** (*right*) species illustrating the stacking (**A1**) interactions (*top*) and intercolumnar (*bottom*) contacts (**A2**-**A4**). For simplicity, all six molecules are noted by the numbering from **M1** to **M6**

Intermolecular interactions in the A1 dimer of the C1 and C2 compounds

Figure 2 show that the C···C, C···S and C···Se interactions provide the intermolecular binding between the stacked molecules. The presence of the definite number of critical points CP(3, −1) for each pair of collinear atoms in the molecular stack indicates the local points in which the potential energy density $\nu(\mathbf{r})$ is decreased [27]. There are no other criss-cross bond pathes with the CP(3, −1) critical points. Thus, the total binding energy of the dimer A1 is determined by formation of a number of the C···C and C···S (C···Se) interactions. The existence of the C···C and C···S contacts for the C1 compound has been confirmed by the precision X-ray experiment [20]. The topological parameters of these contacts have been measured from X-ray and their energies were estimated by the Espinosa equation in ref [20]. The calculated and experimental topological parameters are compared in Table 1. All contacts of the C···C type are characterized by the low electron density $\rho(\mathbf{r})$ values in the bond critical points. The values of the electron density Laplacian are also small and positive which is typical for the closed shell interactions [28]. The kinetic energy density $g(\mathbf{r})$ prevails over the potential energy density $\nu(\mathbf{r})$ in the corresponding bond critical point. It provides a positive values of the electronic energy density $h(\mathbf{r})$ [29], which also indicates the closed-shell type of the C···C interactions. Based on the QTAIM data analysis we predict an existence of additional C(5)···C(6) stacking interaction which is not detected in ref [20]. It should be noted that all C···C bonds (especially C(3)···C(4) for the **C1** compound) are characterized by a high ellipticity values, which suggests their dynamic instability. The energy of C···C interactions calculated with the Espinosa equation (1) are in the range from −0.74 to −0.76 kcal mol^{-1}, which agree well with the reference values [20] for **A1** dimer of the **C1** compound. For the **C2** compound the C···C contacts are a bit weaker (Table 1).

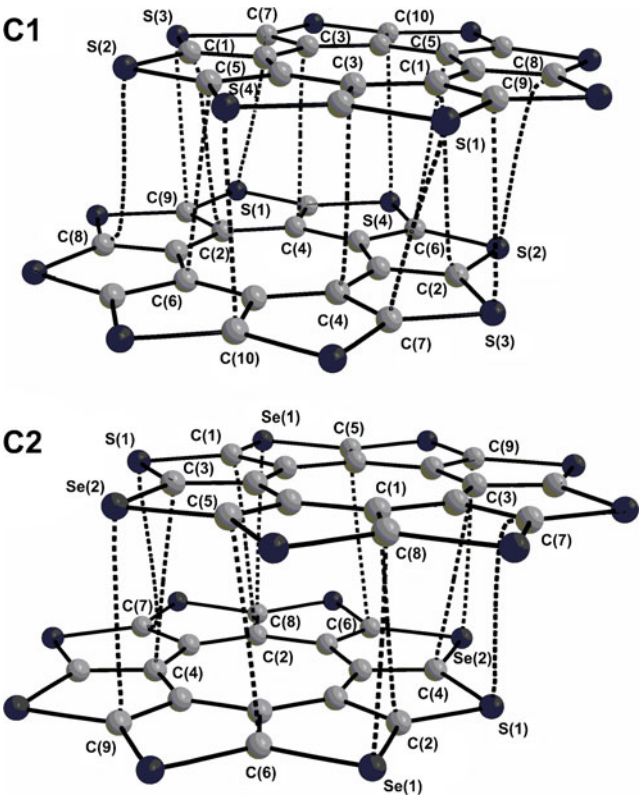

Fig. 2 The structure of the **A1** type dimer containing the stacking interactions

There are four different types of C···S intermolecular bonds in **A1** dimer of the **C1** compound (Fig. 2, Table 1). Unlike, only the single type of C···S contacts exist in the **A1** dimer of the **C2** compound (Table 1). Based on the Laplacian signs and the electron energy density in the corresponding critical point (3, –1), all the C···S bonds should be assigned to

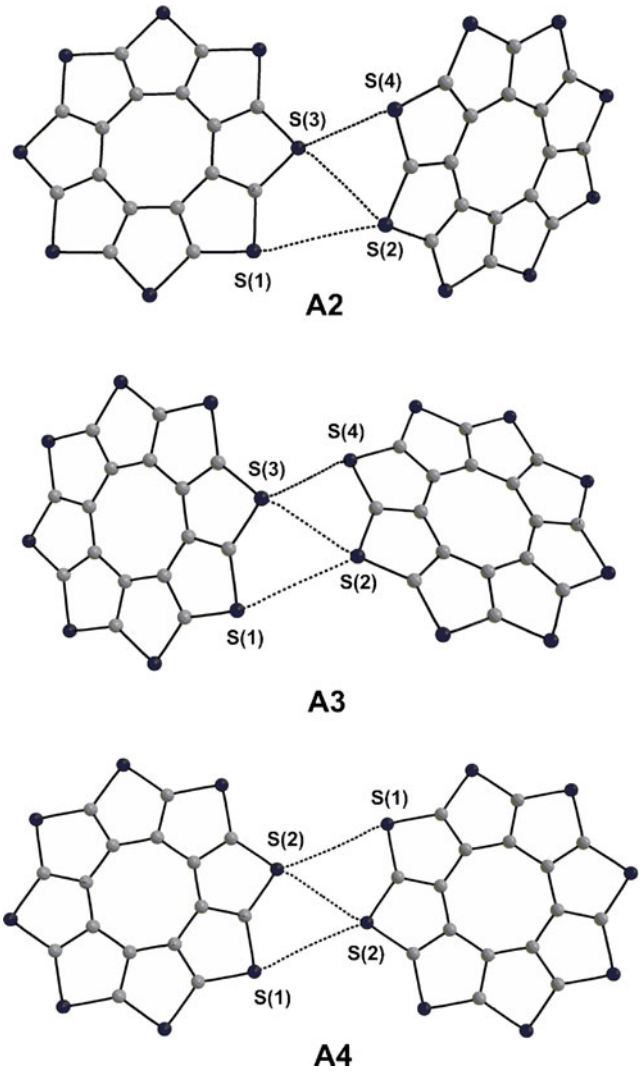

Fig. 3 The structure of the **A2**-**A4** type of dimers containing intermolecular interactions between the **C1** molecules

a closed shell type of interaction ($\nabla^2\rho(\mathbf{r})>0$, $h_e(\mathbf{r})>0$). The calculated energy of C···S bonds is in the range of −0.84 to −1.10 kcal mol^{-1} for the **A1** dimer of the **C1** compound. Doubly degenerate C···S bond in the **A1** dimer of the **C2** compound has a bit lower energy (−0.77 kcal mol^{-1}) due to the larger interatomic distance (Table 1). All C···S contacts are dynamically unstable due to the high bond ellipticity [30] values being similar to C···C contacts. The C···Se contacts in the **A1** dimer of the **C2** compound are very similar by energy and by topological parameters to the C···S interactions in the analogous dimer of the **C1** compound.

In conclusion, it should be noted that all C···C, C···S and C···Se interactions belong to weak van-der-Waals type of contacts which stabilize the **A1** dimer of the **C1** and **C2** compounds by −12.25 and −9.68 kcal mol^{-1}, respectively (Table 2). The intermolecular binding energy estimated by M06-2x/6-31+G(d,p) method in ref [18] is equal to −22.52 kcal mol^{-1} which is almost twice as much as our predictions. This difference in the estimated energies is difficult to explain because the calculation algorithm is not specified in ref [18]. It is also unknown, does the −22.52 kcal mol^{-1} value include the BSSE and ZPE corrections. Additionally, the binding energy from the direct DFT calculations strongly depends on the part of non-local Hartree-Fock exchange in the exchange-correlation functional [41]. For the M06-2X functional the part of HF exchange is equal to 54 %, whereas B3LYP consists of only 20 % of HF exchange. Thus, the "-22.52 kcal mol^{-1}" value depends on the functional and is not experimentally observable for the real crystal (there are different intercolumnar interactions and it is impossible to extract a particular A1 type of dimer from lattice energy) in contrast to the $\nu(\mathbf{r})$ values, which are experimentally measured with a reliable accuracy on the basis of the Abramov's gradient decomposition [42] and local virial theorem:

$$g(\mathrm{r}) = \frac{3}{10}\left(3\pi^2\right)^{\frac{2}{3}}\rho(\mathrm{r})^{\frac{5}{3}} + \frac{1}{6}\nabla^2\rho(\mathrm{r}), \quad (2)$$

$$\nu(\mathrm{r}) = -\frac{3}{5}\left(3\pi^2\right)^{\frac{2}{3}}\rho(\mathrm{r})^{\frac{5}{3}} - \frac{1}{12}\nabla^2\rho(\mathbf{r}), \quad (3)$$

where $\rho(\mathbf{r})$ and $\nabla^2\rho(\mathbf{r})$ values are experimentally measured by the precision X-ray diffraction analysis. Bukalov et al. [20] does not directly determine the total binding energy for the A1 dimer, but the lattice energy value was additively estimated using the Espinosa equation. This energy is equal to −28.5 kcal mol^{-1} with the overall 88 % contribution from the S···S and S···C interactions. It includes intercolumnar interactions which are stronger than stacking interactions in the dimer. Therefore the value "-22.52 kcal mol^{-1}" is definitely overestimated.

Intermolecular interactions in the A2-A4 dimers of the C1 and C2 compounds

The intermolecular bonds in the **A2**-**A4** dimers (Figs. 3 and 4) provide the structural rigidity of the molecular stacks. These contacts are like struts that hold stacked "molecular towers". In the **C1** crystal packing only S···S type of intercolumnar contacts exist (Fig. 3, Table 1). The estimated energy values of this bonds are varied in the range from −0.44 to −2.54 kcal mol^{-1}, i.e., most S···S interactions are slightly stronger than stacking contacts in the A1 dimer. All S···S contacts can be classified as the closed-shell type interactions (the electron energy density and the Laplacian value in the critical point (3, −1) are positive).

As can be seen from Table 1 the topological parameters of the electron density function in the S···S bond CPs demonstrate an excellent agreement with experiment in all details. In addition, we predict an existence of two new very weak S(1)···S(2) bonds in the **A3** and **A4** dimers in addition to

Table 1 Selected parameters of non-covalent interactions in the **C1** and **C2** compounds

Type of contact[a]	Bond	n[b]	d, Å	$\rho(\mathbf{r})$, $a\cdot Å^{-3}$	$\nu(\mathbf{r})$, *a.u.*	$h_e(\mathbf{r})$, *a.u.*	$\nabla^2\rho(\mathbf{r})$, $e\cdot Å^{-5}$	ε	E, *kcal* mol^{-1}
octathio[8]circulene (**C1**)									
A1	C(1)···C(2)	2	3.582	0.031	−0.00234	0.00053	0.33	0.57	−0.74
				0.043[c]	−0.00258[c]		0.38[c]		−0.81[c]
	C(3)···C(4)	2	3.508	0.032	−0.00236	0.00061	0.35	10.38	−0.74
				0.043[c]	−0.00255[c]		0.38[c]		−0.81[c]
	C(5)···C(6)	2	3.526	0.033	−0.00241	0.00056	0.34	1.61	−0.76
	C(7)···S(1)	2	3.653	0.037	−0.00267	0.00074	0.40	0.89	−0.84
				0.042[c]	−0.00260[c]		0.40[c]		−0.82[c]
	C(8)···S(2)	2	3.653	0.040	−0.00284	0.00076	0.42	1.84	−0.89
				0.048[c]	−0.00306[c]		0.45[c]		−0.96[c]
	C(9)···S(3)	2	3.519	0.048	−0.00340	0.00082	0.49	0.14	−1.07
				0.051[c]	−0.00332[c]		0.48[c]		−1.04[c]
	C(10)···S(4)	2	3.511	0.050	−0.00351	0.00083	0.50	0.22	−1.10
				0.051[c]	−0.00335[c]		0.49[c]		−1.05[c]
A2	S(1)···S(2)	1	3.892	0.024	−0.00139	0.00085	0.30	0.16	−0.44
				0.031[c]	−0.00172[c]		0.29[c]		−0.54[c]
	S(2)···S(3)	1	3.501	0.054	−0.00402	0.00140	0.66	0.34	−1.26
				0.062[c]	−0.00435[c]		0.59[c]		−1.36[c]
	S(3)···S(4)	1	3.540	0.055	−0.00404	0.00142	0.66	0.42	−1.27
				0.065[c]	−0.00469[c]		0.63[c]		−1.47[c]
A3	S(1)···S(2)	1	3.722	0.034	−0.00221	0.00113	0.43	0.42	−0.69
	S(2)···S(3)	1	3.512	0.052	−0.00383	0.00136	0.63	0.08	−1.20
				0.057[c]	−0.00384[c]		0.53[c]		−1.20[c]
	S(3)···S(4)	1	3.187	0.089	−0.00811	0.00150	1.07	0.14	−2.54
				0.096[q]	−0.00796[c]		0.92[c]		−2.5[c]
A4	S(1)···S(2)	2	3.903	0.022	−0.00128	0.00084	0.29	0.55	−0.40
	S(2)···S(2)	1	3.321	0.067	−0.00559	0.00156	0.84	0.26	−1.75
				0.073[c]	−0.00546[c]		0.70[c]		−1.71[c]
sym-tetraselenatetrathio[8]circulene (C2)									
A1	C(1)···C(2)	2	3.636	0.028	−0.00207	0.00050	0.297	3.65	−0.65
	C(3)···C(4)	2	3.621	0.028	−0.00200	0.00052	0.292	3.71	−0.63
	C(5)···C(6)	2	3.624	0.030	−0.00228	0.00046	0.309	4.07	−0.72
	C(7)···S(1)	2	3.720	0.036	−0.00244	0.00072	0.374	2.54	−0.77
	Se(1)···C(8)	2	3.605	0.048	−0.00324	0.00072	0.451	0.23	−1.01
	Se(2)···C(9)	2	3.577	0.051	−0.00340	0.00075	0.473	0.28	−1.07
A2	S(1)···S(2)	1	3.753	0.032	−0.00203	0.00106	0.399	0.27	−0.64
	Se(1)···Se(2)	1	3.585	0.061	−0.00364	0.00120	0.583	0.04	−1.14
	S(2)···Se(2)	1	3.247	0.090	−0.00718	0.00154	0.989	0.16	−2.25
A3	S(1)···Se(1)	1	3.908	0.029	−0.00167	0.00075	0.306	0.10	−0.53
	S(2)···Se(2)	1	3.616	0.056	−0.00359	0.00126	0.589	0.37	−1.13
	Se(3)···Se(3)	1	3.578	0.063	−0.00386	0.00124	0.611	0.20	−1.21
A4	S(1)···Se(1)	2	3.879	0.026	−0.00150	0.00082	0.303	0.07	−0.47
	S(1)···S(1)	1	3.326	0.067	−0.00551	0.00153	0.826	0.24	−1.73

[a] **A1**=**M1M2**, **M5M6**; **A2**=**M1M4**, **M2M3**, **M3M6**, **M4M5**; **A3**=**M1M3**, **M2M4**, **M5M3**, **M6M4**; **A4**=**M3M4**

[b] n number of equivalent bonds in the corresponding dimer;

[c] Experimental high-resolution XRD data [20]

Table 2 Total energy (kcal mol^{-1}) of intermolecular interactions estimated by Espinosa's correlation scheme for the different **C1** and **C2** associates in the crystal packing

Compound	A1	A2	A3	A4	hexamer[a]
C1	−12.25 −22.52[b]	−2.97 −2.19[b]	−4.44 −2.06[b]	−2.56 −1.39[b]	−56.70
C2	−9.68	−4.03	−2.86	−2.67	−49.59

[a] Molecular hexamers of **C1** and **C2** are presented in Fig. 1

[b] The binding energy calculated at M06-2X/6-31+G(d,p) level [18]

results of ref [20] (Fig. 3). In the outer perimeter of the **C2** molecule the sulfur and selenium atoms are alternated one by one. Therefore the three different types of interactions (S···S, S···Se and Se···Se) do exist. All of them are similar to the analogous S···S contacts in the **C1** crystal packing (Fig. 4). However, in general a small decrease in the absolute values of $\rho(\mathbf{r})$, $\nabla^2\rho(\mathbf{r})$ and of related parameters is observed due to the larger interatomic distances (Table 1). The total intermolecular stabilization energy of the **A2**-**A4** dimers for both compounds is presented in Table 2. For the **C1** compound the intermolecular binding energies are close similar to the previous predictions on the basis of DFT/M06-2x calculations [18]. For the **C2** compound the stabilization energy of the **A2** and **A3** dimers is close to the same values for the **A**3 and **A2** dimers of the **C1** compound, respectively. Taking into account that the studied molecular hexamers presented in Fig. 1 consist of a number of the same dimers the total estimated intermolecular stabilization energy of the hexamers is equal to −56.70 and −49.59 kcal mol^{-1} for the **C1** and **C2** compounds, respectively. Thus it is logical, that the monocrystalline **C1** compound with the stronger intermolecular stabilization has a red color, while the **C2** compound with more friable crystal packing is colorless.

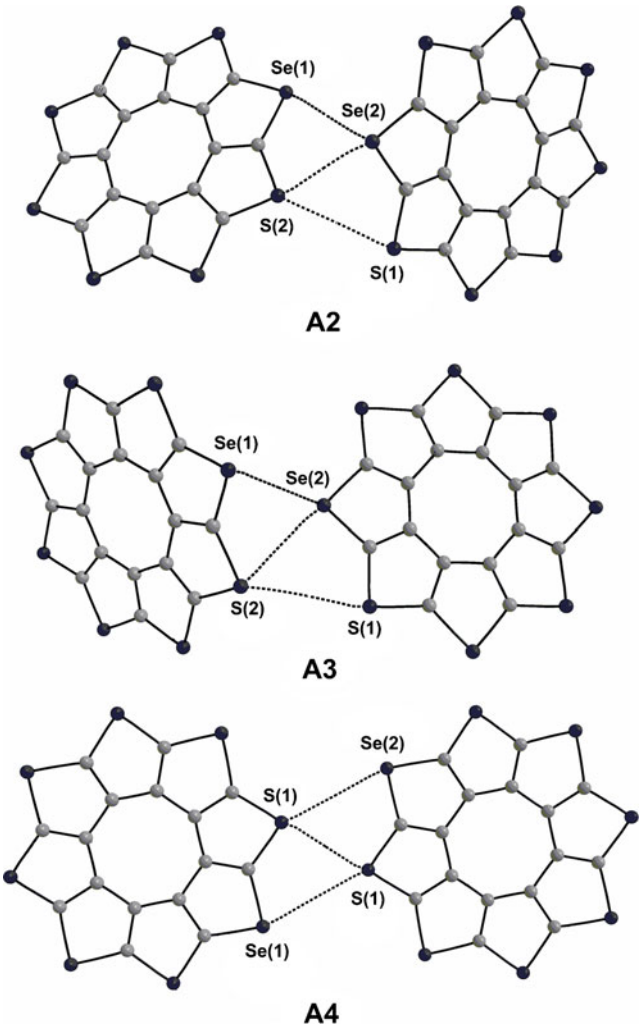

Fig. 4 The structure of the **A2**-**A4** type of dimers containing intermolecular interactions between the **C2** molecules

The adsorption spectra of C1 and C2 compounds

In this section we discuss the absorption spectra of the **C1** and **C2** compounds with their possible symmetry constrains (D_{8h} and D_{4h} for **C1** and **C2** respectively). Because of such high symmetry a large number of the singlet-singlet electronic transitions are forbidden by symmetry criterion. Thus, the first 23 excited singlet states of the **C1** compound are not accessible from the ground state in the electric dipole approximation. The first symmetry allowed singlet-singlet electronic excitation corresponds to the doubly degenerate $X^1A_{1g}\rightarrow{}^1E_{1u}$ vertical transition to the S_{24} and S_{25} electronic states. All low-lying electronic transitions are forbidden but some of them ($S_0\rightarrow S_{12,13}$ and $S_0\rightarrow S_{20,21}$) of the $X^1A_{1g}\rightarrow{}^1E_{1g}$ type are allowed in the magnetic dipole approximation and are polarized in the molecular plane (XY). The most intense $X^1A_{1g}\rightarrow{}^1E_{1u}$ electronic transition for the **C1** molecule ($S_0\rightarrow S_{46,47}$) is predicted at 238.5 nm and provides a strong absorption band in the absorption spectrum of the amorphous octathio[8]circulene with the experimental maximum being at 244 nm [20]. Other allowed singlet-singlet transitions are low-intense and are overlapped by the strong band (Table 3); they form a long-wave shoulder of the main band. However, the vibronic effects in the **C1** molecule may enhance intensity of these weak electronic transitions.

The phosphorescence of the **C1** compound at the ground state geometry is predicted in the visible region at 421 nm. The corresponding $X^1A_{1g}\leftarrow{}^3A_{2g}$ transition is forbidden even with account of spin-orbit coupling and can be induced by spin-vibronic perturbation [43–46].

It is important to note that the lowest lying singlet excited state $^1E_{3g}$ is doubly-degenerate at the ground state geometry. According to Jahn-Teller theorem [47] it should be distorted to the low-symmetry configuration and can provide an intense fluorescence by intensity borrowing through the deformation ungerade vibrations.

Table 3 Absorption properties of the **C1** and **C2** compounds calculated by the TD DFT/B3LYP/6-31G(d) method

ESN[a]	Transition	Deg.	λ, nm	*f*	Assignment
octathio[8]circulene (**C1**)					
$\mathbf{T_1}$	$X^1A_{1g}\rightarrow{}^3B_{1g}$	1	421.0	0.0000	HOMO1→LUMO+2 (32 %) HOMO→LUMO+3 (32 %)
$\mathbf{T_{2,3}}$	$X^1A_{1g}\rightarrow{}^3E_{1u}$	2	401.0	0.0000	HOMO→LUMO (36 %) HOMO-1→LUMO (20 %); HOMO-1→LUMO (36 %) HOMO→LUMO (20 %)
$\mathbf{S_{1,2}}$	$X^1A_{1g}\rightarrow{}^1E_{3u}$	2	314.9	0.0000	HOMO-1→LUMO+1(+73 %) HOMO→LUMO+1(+22 %); HOMO→LUMO+1(+73 %) HOMO-1→LUMO+1(22 %)
$\mathbf{S_{24,25}}$	$X^1A_{1g}\rightarrow{}^1E_{1u}$	2	262.1	0.0664	HOMO-3→LUMO+2 (34 %) HOMO-2→LUMO+3 (34 %); HOMO-3→LUMO+3 (34 %) HOMO-2→LUMO+2 (34 %)
$\mathbf{S_{28}}$	$X^1A_{1g}\rightarrow{}^1A_{2u}$	1	260.4	0.0002	HOMO-1→LUMO+11(36 %) HOMO→LUMO+12 (36 %)
$\mathbf{S_{42}}$	$X^1A_{1g}\rightarrow{}^1A_{2u}$	1	239.2	0.0019	HOMO-2→LUMO+4(41 %) HOMO-3→LUMO+5 (41 %)
$\mathbf{S_{46,47}}$	$X^1A_{1g}\rightarrow{}^1E_{1u}$	2	238.5	0.8348	HOMO-1→LUMO+7 (22 %) HOMO→LUMO+8 (22 %); HOMO-1→LUMO+8 (22 %) HOMO→LUMO+7 (22 %)
$\mathbf{S_{60}}$	$X^1A_{1g}\rightarrow{}^1A_{2u}$	1	223.0	0.0005	HOMO-4→LUMO+6 (87 %) HOMO-1→LUMO+11 (6 %)
sym-tetraselenatetrathio[8]circulene (**C2**)					
$\mathbf{T_1}$	$X^1A_{1g}\rightarrow{}^3A_{2g}$	1	433.4	0.0000	HOMO-1→LUMO+2(31 %) HOMO→LUMO+1(+31 %)
$\mathbf{T_{2,3}}$	$X^1A_{1g}\rightarrow{}^3E_u$	2	414.4	0.0000	HOMO→LUMO (+58 %) HOMO-4→LUMO+1 (19 %); HOMO-1→LUMO (+58 %) HOMO-4→LUMO+2 (+19 %)
$\mathbf{S_{1,2}}$	$X^1A_{1g}\rightarrow{}^1E_g$	2	309.1	0.0000	HOMO-1→LUMO+3 (+65 %) HOMO→LUMO+3 (+24 %); HOMO→LUMO+3 (+65 %) HOMO-1→LUMO+3 (24 %)
$\mathbf{S_{3,4}}$	$X^1A_{1g}\rightarrow{}^1E_u$	2	307.6	0.0025	HOMO-1→LUMO(+77 %) HOMO→LUMO(15 %); HOMO→LUMO(+77 %) HOMO-1→LUMO(+15 %)
$\mathbf{S_{18,19}}$	$X^1A_{1g}\rightarrow{}^1E_u$	2	277.4	0.0265	HOMO-2→LUMO+1(+77 %) HOMO-3→LUMO+2(+16 %); HOMO-2→LUMO+2(+77 %) HOMO-3→LUMO+1(16 %)
$\mathbf{S_{23,24}}$	$X^1A_{1g}\rightarrow{}^1E_u$	2	270.6	0.0130	HOMO-1→LUMO+8(+33 %) HOMO→LUMO+8(+22 %); HOMO→LUMO+8(+33 %) HOMO-1→LUMO+8(22 %)
$\mathbf{S_{29,30}}$	$X^1A_{1g}\rightarrow{}^1E_u$	2	264.7	0.0796	HOMO-1→LUMO+10(+39 %) HOMO-3→LUMO+2(+36 %); HOMO→LUMO+10(+39 %) HOMO-3→LUMO+1(+36 %)
$\mathbf{S_{48,49}}$	$X^1A_{1g}\rightarrow{}^1E_u$	2	244.5	0.7511	HOMO-1→LUMO+10(+50 %) HOMO→LUMO+8(20 %); HOMO→LUMO+10(+50 %) HOMO-1→LUMO+8(+20 %)
$\mathbf{S_{51}}$	$X^1A_{1g}\rightarrow{}^1A_{2u}$	1	242.5	0.0016	HOMO-4→LUMO+5(+61 %) HOMO-2→LUMO+9(33 %)

[a] *ESN* excited state number

The UV absorption properties of the **C2** molecule are quite similar to those of the **C1** compound due to the close similarity of their orbitals energy and nature (Fig. 5), but the presence of the heavy Se atom promotes the bathochromic shift of absorption bands. This is due to the fact that two degenerate highest occupied *eg* orbitals of the **C2** molecule have a higher energy than the analogous *e3g* orbitals of the **C1** molecule. At the same time the energies of the lowest unoccupied *a2u* molecular orbital for both compounds are very similar; this provides finally the red shift of the corresponding electronic transitions. The most intense absorption band for the **C2** compound is calculated at 244.5 nm and the first allowed $X^1A_{1g}\rightarrow{}^1E_u$ electronic transition is predicted at 307.6 nm. In general, the UV absorption spectra of the **C1** and **C2** compounds is formed by doubly degenerate $X^1A_{1g}\rightarrow{}^1E_{1u}$ and $X^1A_{1g}\rightarrow{}^1E_u$ type excitations, respectively. The electronic transitions of the $X^1A_{1g}\rightarrow{}^1A_{2u}$ symmetry for both compounds are characterized by much weaker intensity; they are perpendicularly polarized and determined by $\pi\rightarrow\sigma^*$ excitations [48, 49]. These

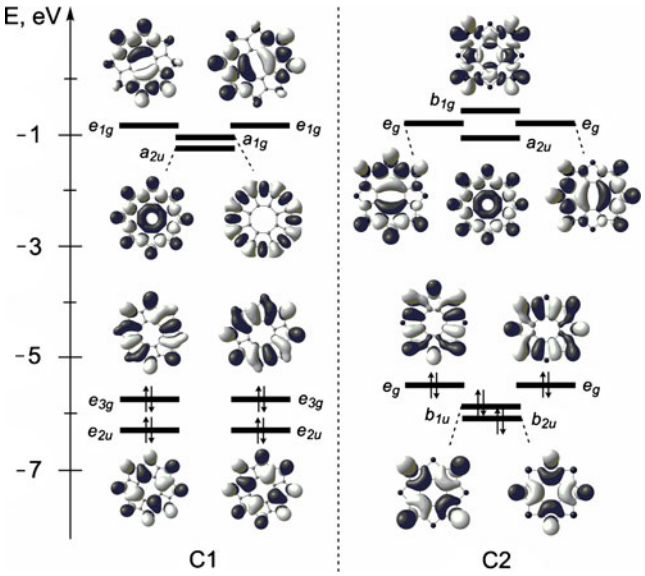

Fig. 5 The energy diagram of the frontier molecular orbitals of the **C1** and **C2** compounds (the control iso-density value is equal to 0.02 a.u.)

transitions are overlapped by more intense transitions to the $^1E_{1u}$ and ^1E_u electronic states.

Thus, we can conclude that the **C1** and **C2** compounds are colorless if we consider the absorption spectra of single molecules in a gas phase.

It is important to stress, that the **C1** single crystal has a red color [20]. Awaga et al. [15] have proposed that the red color of the **C1** compound is probably caused by an interference effect due to the film thickness of 500 nm, which is comparable with the visible light wavelengths. However, at the same time, Bukalov et al. [20] have found the **C1** single crystals of the 10 μ thickness are also red. This can not be explained by an interference effect and was tentatively interpreted [20] by strong intermolecular interaction in the crystal. Indeed, the **C1** crystal is very stable and constitutes a long red needle. In contrast, the molecular layers for the **C2** compound are more friable, the needles are short and **C2** crystals are colorless.

Conclusions

The QTAIM study of the octathio[8]circulene and *sym*-tetraselenatetrathio[8]circulene species permits us to determine the direct correlation between the single crystal architecture and the absorption spectra of the studied molecules. On the basis of QTAIM approach we have detected some new intermolecular bonds for the **C1** dimer compounds, such as the C(5)···C(6) for the **A1** contact and the S(1)···S(2) bond for the **A3** and **A4** contacts which have been missed previously [20]. The topological analysis for the different **C2** dimers has been presented here for the first time.

The intermolecular non-covalent interactions in the **C1** and **C2** compound are strong enough for indication of the frontier orbitals splitting. The total energy of intermolecular bonds for the **C1** hexamer is higher than those for the **C2** hexamer. Thus, the **C1** single crystals have a red color and C2 single crystals are colorless. At the same time a chaotic disposition of the **C1** and **C2** molecules in the amorphous phase does not lead to the color appearance.

References

1. Chernichenko KY, Sumerin VV, Shpanchenko RV, Balenkova ES, Nenajdenko VG (2006) "Sulflower": a new form of carbon sulfide. Angew Chem Int Ed 118:7527–7530
2. Ivasenko O, MacLeod JM, Chernichenko KYu, Balenkova ES, Shpanchenko RV, Nenajdenko VG, Rosei F, Perepichka DF (2009) Supramolecular assembly of heterocirculenes in 2D and 3D. Chem Commun doi: 10.1039/b819532c
3. Dadvand A, Cicoira F, Chernichenko KYu, Balenkova ES, Osuna RM, Rosei F, Nenajdenko VG, Perepichka DF (2008) Heterocirculenes as a new class of organic semiconductors. Chem Commun doi: 10.1039/b809259a
4. Chernichenko KY, Balenkova ES, Nenajdenko VG (2008) From thiophene to sulflower. Mendeleev Commun 18:171–179
5. Erdtman H, Hogberg HE (1968) Tetranaphthocyclo-octatetraene tetra-oxide, a cyclisation product from α-naphthoquinone. Chem Commun (London) pp 773–774
6. Nielsen CB, Brock-Nannestad T, Reenberg TK, Hammershøj P, Christensen JB, Stouwdam JW, Pittelkow M (2010) Organic light-emitting diodes from symmetrical and unsymmetrical π-extended tetraoxa[8]circulene. Chem Eur J 16:13030–13034
7. Nielsen CB, Brock-Nannestad T, Hammershøj P, Reenberg TK, Schau-Magnussen M, Trpcevski D, Salcedo R, Baryshnikov GV, Minaev BF, Pittelkow M (2013) Azatrioxa[8]circulenes: planar anti-aromatic cyclooctatetraenes. Chem Eur J 19:3898–3904
8. Baryshnikov GV, Minaev BF, Minaeva VA, Baryshnikova AT, Pittelkow M (2012) DFT and QTAIM study of the tetra-tert-butyltetraoxa[8]circulene regioisomers structure. J Mol Struct 1026:127–132
9. Minaeva VA, Minaev BF, Baryshnikov GV, Agren H, Pittelkow M (2012) Experimental and theoretical study of IR and Raman spectra of tetraoxa[8]circulenes. Vib Spectrosc 61:156–166
10. Minaeva VA, Minaev BF, Baryshnikov GV, Romeyko OM, Pittelkow M (2013) The FTIR spectra of substituted tetraoxa[8]circulenes and their assignments based on DFT calculations. Vib Spectrosc 65:147–158
11. Baryshnikov GV, Minaev BF, Pittelkow M, Nielsen CB, Salcedo R (2013) Nucleus-independent chemical shifts criterion of aromaticity in the π-extended tetraoxa[8]circulenes. J Mol Model 19:847–850
12. Minaev BF, Baryshnikov GV, Minaeva VA (2011) Density functional theory study of electronic structure and spectra of tetraoxa[8]circulenes. Comput Theor Chem 972:68–74
13. Minaeva VA, Minaev BF, Baryshnikov GV, Romeyko ON, Pittelkow M (2012) Raman spectra of tetraoxa[8]circulenes. *p*-dinaphthalenodiphenylenotetrafuran and its tetraalkyl derivatives (DFT study and experiment). J Appl Spectrosc 79:695–707
14. Takuya F, Michio MM, Awaga K (2009) Electrochemical field-effect transistors of octathio[8]circulene robust thin films with ionic liquids. Chem Phys Lett 483:81–83
15. Fujimoto T, Matsushita MM, Yoshikawa H, Awaga K (2008) Electrochemical and electrochromic properties of octathio[8]circulene thin films in ionic liquids. J Am Chem Soc 130:15790–15791
16. Gahungu G, Zhang J (2008) Shedding light on octathio[8]circulene and some of its plate-like derivatives. Phys Chem Chem Phys 10:1743–1747
17. Mohakud S, Pati SK (2009) Large carrier mobilities in octathio[8]circulene crystals: a theoretical study. J Mater Chem 19:4356–4361
18. Tang X-D, Liao Y, Gao H-Z, Geng Y, Su Z-M (2012) Theoretical study of the bridging effect on the charge carrier transport properties of cyclooctatetrathiophene and its derivatives. J Mater Chem 22:6907–6918
19. Fujimoto T, Matsushita MM, Awaga K (2010) Dual-gate field-effect transistors of octathio[8]circulene thin-films with ionic liquid and SiO2 gate dielectrics. Appl Phys Lett 97:123303
20. Bukalov SS, Leites LA, Lyssenko KA, Aysin RR, Korlyukov AA, Zubavichus JV, Chernichenko KY, Balenkova ES, Nenajdenko VG, Antipin MY (2008) Two modifications formed by "sulflower" $C_{16}S_8$ molecules, their study by XRD and optical spectroscopy (Raman, IR, UV–vis) methods. J Phys Chem A 112:10949–10961
21. Fujimoto T, Suizu R, Yoshikawa H, Awaga K (2008) Molecular, crystal, and thin-film structures of octathio[8]circulene: release of antiaromatic molecular distortion and lamellar structure of self-assembling thin films. Chem Eur J 14:6053–6056
22. Aragó J, Viruela PM, Ortí E (2009) From linear quaterthiophene to sulflower: a comparative theoretical study. J Mol Struct (THEOCHEM) 912:27–31
23. Becke AD (1993) Density functional thermochemistry. III. The role of exact exchange. J Chem Phys 7:5648–5652

24. Lee C, Yang W, Parr RG (1988) Development of the Colle-Salvetti correlation-energy formula into a functional of the electron density. Phys Rev B 37:785–789
25. Francl MM, Petro WJ, Hehre WJ, Binkley JS, Gordon MS, DeFrees DJ, Pople JA (1982) Self-consistent molecular orbital methods. XXIII. A polarization type basis set for second-row elements. J Chem Phys 77:3654–3665
26. Frisch M, Trucks G, Schlegel H, Scuseria G, Robb M, Cheeseman J, Montgomery J, Vreven J, Kudin K, Burant J, Millam J, Iyengar S, Tomasi J, Barone V, Mennucci B, Cossi M, Scalmani G, Rega N, Petersson G, Nakatsuji H, Hada M, Ehara M, Toyota K, Fukuda R, Hasegawa J, Ishida M, Nakajima T, Honda Y, Kitao O, Nakai H, Klene M, Li X, Knox RJ, Hratchian H, Cross J, Bakken V, Adamo C, Jaramillo J, Gomperts R, Stratmann R, Yazyev O, Austin A, Cammi R, Pomelli C, Ochterski J, Ayala P, Morokuma K, Voth G, Salvador P, Dannenberg J, Zakrzewski V, Dapprich S, Daniels A, Strain M, Farkas O, Malick D, Rabuck A, Raghavachari K, Foresman J, Ortiz J, Cui Q, Baboul A, Clifford S, Cioslowski J, Stefanov B, Liu G, Liashenko A, Piskorz P, Komaromi I, Martin R, Fox D, Keith T, Al-Laham M, Peng C, Nanayakkara A, Challacombe M, Gill P, Johnson B, Chen W, Wong M, Gonzalez C, Pople J (2004) Gaussian 03, revision C.02. Gaussian, Inc, Wallingford, CT
27. Bader RFW (1990) Atoms in molecules. A quantum theory. Clarendon, Oxford, U.K
28. Bader RFW, Essen H (1984) The characterization of atomic interactions. J Chem Phys 80:1943–1960
29. Cremer D, Kraka E (1984) Description of the chemical bond in terms of local properties of electron density and energy. Croat Chem Acta 57:1259–1281
30. Bader RFW, See TS, Cremer D, Kraka E (1983) Description of conjugation and hyperconjugation in terms of electron distributions. J Am Chem Soc 105:5061–5068
31. Keith TA (2010) AIMAll (Version 10.07.25), TK Gristmill Software. Overland Park KS, USA, www.aim.tkgristmill.com
32. Bertolotti F, Forni A, Gervasio G, Marabello D, Diana E (2012) Experimental and theoretical charge density of hydrated cupric acetate. Polyhedron 42:118–127
33. Gall V, Breza M (2009) QTAIM study of transition metal complexes with cyclophosphazene-based multisite ligands I: Zinc(II) and Nickel(II) complexes. Polyhedron 28:521–524
34. Rybalova TV, Bagryanskaya IY (2009) C-F…π, F…H, and F…F intermolecular interactions and F-aggregation: role in crystal engineering of fluoroorganic compounds. J Struct Chem 50:741–753
35. Espinosa E, Molins E, Lecomte C (1998) Hydrogen bond strengths revealed by topological analyses of experimentally observed electron densities. Chem Phys Lett 285:170–173
36. Espinosa E, Alkorta I, Rozas I, Elguero J, Molins E (2001) About the evaluation of the local kinetic, potential and total energy densities in closed-shell interactions. Chem Phys Lett 336:457–461
37. Latosińska N, Latosińska M, Tomczak MA, Seliger J, Žagar V (2011) Supramolecular synthon pattern in solid clioquinol and cloxiquine (APIs of antibacterial, antifungal, antiaging and antituberculosis drugs) studied by ^{35}Cl NQR, ^{1}H-^{17}O and ^{1}H-^{14}N NQDR and DFT/QTAIM. J Mol Model 17:1781–1800
38. Nguyen TH, Groundwater PW, Platts JA, Hibbs DE (2012) Experimental and theoretical charge density studies of 8-hydroxyquinoline cocrystallized with salicylic acid. J Phys Chem A 116:3420–3427
39. Shishkina AV, Zhurov VV, Stash AI, Vener MV, Pinkerton AA, Tsirelson VG (2013) Noncovalent interactions in crystalline picolinic acid N-oxide: insights from experimental and theoretical charge density analysis. Cryst Growth Des 13:816–828
40. Runge E, Gross EKU (1984) Density-functional theory for time-dependent systems. Phys Rev Lett 52:997–1000
41. González Moa MJ, Mandado M, Mosquera RA (2007) A computational study on the stacking interaction in quinhydrone. J Phys Chem A 111:1998–2001
42. Abramov YA (2007) On the possibility of kinetic energy density evaluation from the experimental electron-density distribution. Acta Crystallogr A 53:264–272
43. Minaev BF (2007) Electronic mechanisms of molecular oxygen activation. Russ Chem Rev 76:989–1011
44. Minaev BF (2005) Intensity of singlet–triplet transitions in C_{60} fullerene calculated on the basis of the time-dependent density functional theory and taking into account the quadratic response. Opt Spectrosc 98:336–340
45. Minaev BF, Minaev AB (2005) Calculation of the phosphorescence of porphyrins by the density functional method. Opt Spectrosc 98:214–219.
46. Minaev BF (2004) Ab initio study of the ground state properties of molecular oxygen. Spectrochim Acta A 60:1027–1041
47. Jahn HA, Teller E (1937) Stability of polyatomic molecules in degenerate electronic states. I. Orbital degeneracy. Proc Roy Soc 161:220–235
48. Rubio-Pons O, Loboda O, Minaev B, Schimmelpfennig B, Vahtras O, Ågren H (2003) CASSCF calculations of triplet-state properties. Applications to benzene derivatives. Mol Phys 101:2103–2114
49. Minaev BF, Minaeva VA (2001) MCSCF response calculations of the excited states properties of the O_2 moelcule and a part of its spectrum. Phys Chem Chem Phys 3:720–729